Collapse of turbulence in stably stratified channel flow: a transient phenomenon

J.M.M. Donda [(1)], I.G.S. van Hooijdonk[(1)], A.F. Moene[(2)], H.J.J. Jonker[(3)], G.J.F. van Heijst[(1)], H.J.H. Clercx[(1)] and B.J.H. van de Wiel[(1)]

(1) Fluid Dynamics Laboratory and J.M. Burgerscentrum, Eindhoven University of Technology, Eindhoven, Netherlands
(2) Department of Meteorology and Air Quality, Wageningen University, Wageningen, Netherlands
(3) Applied Physics, Delft University of Technology, Delft, Netherlands

The collapse of turbulence in a pressure driven, cooled channel flow is studied by using 3-D direct numerical simulations (DNS) in combination with theoretical analysis using a local similarity model. Previous studies with DNS reported a definite collapse of turbulence in case when the normalized surface cooling h/L (with h the channel depth and L the Obukhov length) exceeded a value of 0.5. A recent study by the present authors succeeded to explain this collapse from the so-called Maximum Sustainable Heat Flux (MSHF) theory. This states that collapse may occur when the ambient momentum of the flow is too weak to transport enough heat downward to compensate for the surface cooling. The MSHF theory predicts that in pressure driven flows, acceleration of the fluid after collapse eventually will cause a regeneration of turbulence, thus in contrast with the aforementioned DNS results. Also it predicts that the flow should be able to survive 'supercritical' cooling rates, in case when sufficient momentum is applied on the initial state. Here, both predictions are confirmed using DNS simulations. It is shown that also in DNS a recovery of turbulence will occur naturally, provided that perturbations of finite amplitude are imposed to the laminarized state and provided that sufficient time for flow acceleration is allowed. As such, it is concluded that the collapse of turbulence in this configuration is a temporary, transient phenomenon for which a universal cooling rate does not exist. Finally, in the present work a one-to-one comparison between a parameterized, local similarity model and the turbulence resolving model (DNS), is made. Although, local similarity originates from observations that represent much larger Reynolds numbers than those covered by our DNS simulations, both methods appear to predict very similar mean velocity (and temperature) profiles. This suggests that in-depth analysis with DNS can be an attractive complementary tool to study atmospheric physics in addition to tools which are able to represent high Reynolds number flows like Large Eddy Simulation.

Key Words: nocturnal boundary layer; direct numerical simulation; collapse of turbulence, revival of turbulence

1. Introduction

In this work a numerical study on a strongly stratified channel flow is performed as an idealized analogy to nocturnal boundary layer flows in conditions of clear skies and weak winds. We build on pioneering work by Nieuwstadt (2005) (herefrom: N05) who studied the collapse of turbulence using Direct Numerical Simulations. In particular, a re-interpretation of Nieuwstadts findings (N05) is made using recent theoretical insights (Van de Wiel et al. (2012); herefrom:VdW12). From this, an intriguing paradox in Nieuwstadts results is solved. It deals with the question if turbulence may or may not recover from an initial collapse as a result of intensive surface cooling. It will be shown that even in the case of extreme cooling, flow acceleration after collapse enables a recovery, provided that sufficiently large perturbations are present to trigger the onset to turbulence.

From literature it is well-known that weak wind conditions favour the occurrence of the so-called very stable atmospheric boundary layer regime (Sun et al. (2012)). As turbulence is weak, intermittent, or virtually absent, fog and frost events may easily occur. As such, a solid physical understanding of this regime is essential for weather forecasting practice (Holtslag et al. (2013)). In contrast to the weakly stable boundary layer, the very stable boundary layer is poorly understood (for a recent review we refer to: Mahrt (2014)). Though from an experimental point of view considerable effort has been made to improve our understanding (e.g. Cuxart et al. (2000); Poulos et al. (2002); Grachev et al. (2005); Hoch and Calanca (2007); Wyngaard (2008); Mahrt (2011); Sun et al. (2012)),)), the number of numerical studies on VSBL dynamics has been limited so far; most of the work has been restricted to the continuously turbulent regime (with exceptions mainly from conceptual studies such as e.g. in McNider et al. (1995), Van de Wiel et al. (2002), Costa et al. (2011), Acevedo et al. (2012) and Łobocki (2013)). In strongly stratified conditions, parametrization of radiative and turbulent transport processes is far from trivial (Edwards (2009)). To a lesser extent this is also true for turbulence resolving models like Large-Eddy Simulation (LES). Although recent success has been reported on the stationary, continuous turbulent case (for an overview see: Beare (2008)), very few studies have reported successful LES simulations on the non-stationary case (interesting exceptions are given in Jimenez and Cuxart (2005); Cuxart and Jimenez (2007); Zhou and Chow (2011); Huang and Bou-Zeid (2013). This is even more true for the 'calm' wind regime where subgrid fluxes tend to dominate over the total such that LES degenerates to its subgrid model, which, in turn, has to rely on a parametrized description of turbulence (see the discussion in Beare (2008)).

Alternatively, Direct Numerical Simulations (DNS) could be used for simulating the transition towards the calm regime. One of the advantages of DNS is that turbulent motions are fully resolved down to the Kolmogorov scale, without the need to invoke a particular turbulence closure model. Also, the appearance of a calm regime will naturally manifest itself as a laminarized state. However, a serious drawback of the DNS method is the fact that only modest Reynolds numbers can be simulated, i.e., low as compared to geophysical values (section 2). This clearly limits the generality of our results. As such, the outcome of studies like the present one can only be complementary to the other SBL-modelling efforts which do represent high Reynolds number flows.

As mentioned above, we depart from the work by Nieustadt (N05) who investigated a pressure-driven stably stratified channel flow by means of Direct Numerical Simulations. Starting from a neutrally stratified situation, suddenly a fixed amount of heat was extracted from the surface. The non-dimensional heat flux was denoted by h/L_{ext}, with h the domain height and L_{ext} the steady-state Obukhov length (section 2). Next, the experiment was repeated for increasing values of h/L_{ext}. Starting from the neutral case ($h/L_{ext} = 0$), the system was able to sustain turbulence until the imposed surface cooling exceeded the critical value of 0.5 (or $h/L_{ext} = 1.23$ if one excludes the Von Kármán constant in the definition of L_{ext} as originally in N05). The system showed a definite collapse of turbulence for a cooling rate above the critical value $h/L_{ext} > 0.5$. Later, this critical value was confirmed by Flores and Riley (2011) (in their definition the Von Kármán constant is used) and they investigated its dependence on the Reynolds number. In both studies, however, a collapse of turbulence appeared to be *permanent*.

Inspired by this, VdW12 simulated the same channel flow using a simple local closure model. The simplicity of the model allowed revealing the physical mechanism behind the collapse based on maximum sustainable heat flux hypothesis. Besides the formal approach in that work, here, we summarize the basic principle by a crudely simplified cartoon (Figure 1). For a given shear, the turbulent heat flux $|H|$ maximizes at moderate stability in stratified flows: the heat flux becomes small in both the neutral limit (small temperature gradient) and the very stable limit (weak mixing). This basic characteristic has been reported in many studies and is readily derived within the framework of local similarity (Taylor (1971); Malhi (1995); Mahrt (1998); Delage et al. (2002); Basu et al. (2006); Sorbjan (2006); Grachev et al. (2005)). The height of the maximum itself strongly depends on the magnitude of the ambient shear. In N05 a prescribed heat flux H_0 is extracted at the surface (dashed line Figure 1). Next, it is clear that in case of strong cooling (H_0) and/or weak winds, the flow is unable to compensate the heat loss at the surface. As such the surface temperature decreases rapidly, which further increases stability. This positive feedback loop leads to strongly suppressed levels of turbulence. Detailed mathematical analysis in VdW12 showed that this feedback is indeed responsible for the eventual collapse in the stratified channel flow.

Next, the question is: what happens after the collapse? Figure 1 is applicable to the case when shear is fixed. In reality, however, the reduced turbulent friction leads to acceleration of the mean flow by the horizontal pressure gradient (the so-called Businger mechanism; Businger (1973)). Therefore, after some time the shear of the flow has largely increased. Following Figure 1 (continuous black line) the heat transport capacity of the flow has increased accordingly, so that this condition for the regeneration of turbulence is fulfilled. Indeed, in VdW12 the local similarity model showed a recovery of turbulence on the long term. So why then, why did such recovery not occur in N05? The present work hypothesizes that the reason lies in the absence of a sufficient trigger mechanism in the DNS simulations. A purely laminar flow could be hydrodynamically stable to infinitesimal perturbations, even in case of sufficient ambient shear (compare Boing et al. (2010)). In reality, however, finite size perturbations are the rule rather than exception. One could think of disturbances generated by small-scale topography, submeso motions or disturbances generated by the internal gravity waves (Mahrt (2014)). Therefore, we will investigate whether it is possible to trigger the flow such that it recovers to a fully turbulent state after the collapse event. In that case the 'supercritical' cooling rate of $h/L_{ext} > 0.5$ by Nieuwstadt, would not be critical in a strict sense (section 4.1).

Another interesting consequence of Figure 1 is that it predicts that the turbulence of the flow could survive the 'critical' cooling rate of $h/L_{ext} = 0.5$, provided that sufficient shear is given to the initial flow. Here, this case will be studied in section 4.2. and it will be shown that the anticipated result occurs: turbulence is sustained. Again, the $h/L_{ext} = 0.5$ criterion for collapse is only valid for the specific case of N05 where a flow with weak shear is supplied as initial condition. Note that the concept of Figure 1, i.e. comparing

H_{max} to H_0 has an equivalent interpretation in terms of velocities. The extracted heat H_0 namely determines a characteristic velocity scale U_{min} (VdW12). As such one can compare the ambient wind U to the minimal wind needed to sustain turbulence U_{min}, using the so-called *shear capacity* U/U_{min}. An initial condition with the *shear capacity* greater than 1 implies presence of sufficient shear to sustain turbulence. This interesting aspect is discussed at length in a separate paper by the present authors (Van Hooijdonk et al. (2014)).

The last question to be addressed in the present paper is connected to the relation between Direct Numerical Simulation and local similarity scaling. As typical Reynolds numbers covered by DNS ($O(10^4)$) are much lower than in outdoor atmospheric flows ($O(10^8)$), it is non-trivial that an analogy would exist. Fortunately, simulations by e.g. Coleman et al. (1992), Van de Wiel et al. (2008), N05 and Ansorge and Mellado (2014) have shown that dimensionless quantities tend to follow local similarity-scaling in accordance with atmospheric observations. However, a one-to-one comparison between DNS and an analytical local similarity model as in the present paper has not been reported. It will be shown that the mean profiles of both models closely correspond (sections 3). Due to this correspondence the analytical model becomes useful as a tool to interpret the DNS results and also as a useful surrogate to predict equilibrium profiles and turbulence energetics (section 4 and 5).

2. A stably stratified channel flow

2.1. *Set-up of Direct Numerical Simulation (DNS)*

In the present study we adopt the stably stratified channel flow configuration of N05. An open channel flow, statistically homogeneous in the horizontal directions, is forced by a horizontal pressure gradient ($\partial P/\partial x$). The pressure gradient is imposed by assigning a value for the friction Reynolds number: $Re_* = u_{*ext}h/\nu = 360$, with h the channel depth and ν the kinematic viscosity of the fluid. By definition, the value of u_{*ext} equals the surface friction velocity u_{*0} in steady state. The subscript 'ext' refers to the fact that external parameters are used for this velocity scale (in contrast to the actual surface friction velocity $u_{*0}(t)$ which varies in time).Here, u_* is written:

$$u_{*ext} = \sqrt{-(1/\rho)(\partial P/\partial x)h}, \tag{1}$$

with ρ the density of the fluid. As initial condition, a fully developed neutral channel flow satisfying $\partial P/\partial x$ is applied. The simulations are performed with a constant time step equal to $\Delta t = 0.0002 t_*$, where t_* is defined as:

$$t_* = \frac{h}{u_{*ext}}. \tag{2}$$

At the lower boundary the amount of heat extracted at the surface, H_0, is prescribed by fixing the external parameter h/L_{ext}, defined as:

$$\frac{h}{L_{ext}} = \frac{\kappa g h}{T_{ref}\rho c_p}\frac{H_0}{u_{*ext}^3}, \tag{3}$$

with κ the Von Kármán constant, g the gravitational acceleration, T_{ref} the reference temperature and c_p the heat capacity of the air at constant pressure. It is important to note that, contrary to N05, we include the Von Kármán constant in the definition of L_{ext}, following meteorological conventions. Thus, our $h/L_{ext} = 0.4$ and $h/L_{ext} = 0.5$ must be compared with the N05 cases $h/L_{ext} = 1$ and $h/L_{ext} = 1.23$.
At the top of the domain ($z = h$), the temperature is fixed at T_{ref} and a free stress condition is imposed ($\partial U/\partial z = 0$). At the bottom, a no-slip boundary condition is applied. Zero vertical velocity is prescribed at the top and at the bottom of the domain. In both horizontal directions periodic boundary conditions are applied. A schematic picture of the configuration is given in Figure 2.

In order to simulate the flow described above, we are using a direct numerical simulation (DNS) code. Implementational details of the model are similar to those of the LES model used in (Moene (2003)): a second-order finite volume discretization in space and the second-order Adams-Bashforth method is used for time integration. For consistency with N05, the Prandtl number ($Pr = \nu/\lambda$) is set to unity, although 0.72 seems more realistic for atmospheric dry air. The computational domain measures $L_h = 5h$ in the horizontal directions and $L_v = h$ in the vertical direction. To assume consistency with the results of N05, we use a 100^3 computational grid in the three orthogonal directions. Note that it is realized that this grid resolution is rather modest given the current computational standards which increased since N05, i.e. the case we aim to mimic here. Nevertheless double resolution checks (200^3) where made by the presents authors in order to perform a sensitivity test (see below). To establish whether a 100^3 grid suffices for DNS of a $Re_* = 360$ flow, we summarize the analysis developed in N05. We consider an equilibrium flow situation and assume that the height-averaged dissipation $\langle\epsilon\rangle$ of the turbulence kinetic energy equals the average shear production:

$$\langle\epsilon\rangle = \frac{1}{h}\int_0^h u_*^2(z)\frac{\partial U}{\partial z}dz = \frac{1}{h}\left[U u_*^2\right]_0^h - \frac{1}{h}\int_0^h U\frac{\partial u_*^2}{\partial z}dz, \tag{4}$$

with u_*^2 the local stress divided by density (the surface value of $u*$ is denoted u_{*0}). The first term at the right hand side drops out and the equilibrium state stress divergence is height-independent:

$$\frac{\partial u_*^2}{\partial z} = \frac{1}{\rho}\frac{\partial P}{\partial x}, \tag{5}$$

so that we obtain an estimate for average dissipation:

$$\langle\epsilon\rangle \approx -\frac{1}{\rho}\frac{\partial P}{\partial x}\langle U\rangle, \tag{6}$$

with $\langle U \rangle$ the height-averaged velocity. From the dissipation rate, the Kolmogorov length scale η is found:

$$\eta = \left(\frac{\langle \epsilon \rangle}{\nu^3} \right)^{-\frac{1}{4}}. \tag{7}$$

It should be stressed that this estimate of η is based on the domain averaged dissipation rate. Close to the surface both shear stress and shear will be relatively large and hence the production and dissipation of the turbulent kinetic energy, resulting in a smaller η. We combine with the definition of Re_* to obtain the ratio between the domain height and the Kolmogorov length:

$$\frac{h}{\eta} = \left(\frac{\langle U \rangle}{u_* ext} Re_*^3 \right)^{-\frac{1}{4}}. \tag{8}$$

With $Re_* = 360$ and a typical value for $\langle U \rangle / u_{*ext} \simeq 20$, we estimate: $h/\eta \simeq 175$. By combining h/η with the number of grid cells $h/\Delta z = 100$, we obtain: $\Delta z/\eta \simeq 1.75$ and $\Delta x/\eta = \Delta y/\eta \simeq 9$. As discussed in N05 this is at the limit of what one could call a DNS, and we accept it for our problem because the effects of static stability manifest themselves at scales much larger than η. Finally, we discuss that a sensitivity test was made by the present authors (Moene et al. (2010)) which showed that 200^3 runs for $Re_* = 360$ lead to very similar results.

2.2. *Collapse of turbulence: is it definite?*

In order to investigate the collapse of turbulence in a stably stratified channel flow, a few cases of N05 were redone to check consistency of the results. As a preliminary test, results from Nieuwstadt's default case ($h/L_{ext} = 0.4$) were compared with the current results with respect to characteristic flow properties like profiles of mean and turbulent quantities. It was found that the results were very similar (see also: Moene et al. (2010)). Here, we focus on the 'critical' cooling rate at which a collapse of turbulence is found to occur. In N05 this collapse occurred at a value $h/L_{ext} \geq 0.5$. In Figure 3, the evolution of non-dimensional turbulent kinetic energy for a number of cases with different surface cooling rates h/L_{ext} is plotted. We observe that up to $h/L_{ext} < 0.5$ the flow is able to reach a steady state after an initial period of adjustment to the new surface boundary condition. On the other hand, for cooling rates $h/L_{ext} \geq 0.5$, the turbulent kinetic energy is rapidly decreasing to a very small value in the interval $0 < t/t_* < 5$. As such, the flow transition at $h/L_{ext} \simeq 0.5$ found by N05 is confirmed. Note that this sudden decrease of turbulent kinetic energy is referred to as the collapse of turbulence (VdW12).

The question is: what happens after the collapse? In the study with the local similarity model of VdW12, the collapse of turbulence implies that the wall-induced friction on the flow is largely reduced. This causes flow acceleration, which, according to the hypothesis in Figure 1, largely increases the maximum heat transport capacity of the flow. In their local similarity model, turbulence is regenerated and due to the enhanced shear the flow is able to compensate the flux demand at the surface. A new equilibrium is reached where also Reynolds stresses compensate the pressure force again. But then why such recovery was not found in the DNS by N05? To solve this paradox two-step approach is taken.

First, a one-to-one comparison between the local similarity model of VdW12 and the DNS mean profiles is made in section 3. To this end an analytical model for the steady state is considered. It will be shown that a rather close correspondence between this analytical model and the DNS profiles is found. This suggests that the maximum sustainable heat flux mechanism may play a dominant role in the DNS-case as well. Another benefit of the analytical approach is that it can be used to predict the turbulent end state of the DNS in case it would recover from collapse (section 4). Finally, analytical solutions will be used to provide alternative initial profiles (apart from the standard neutral profile in N05). The maximum sustainable heat flux hypothesis namely predicts that initial flows with sufficient momentum should be able to survive 'supercritical' cooling rates. In section 4 it will be shown that this is indeed the case.

Next, the DNS simulations of N05 themselves are put in a different perspective. What if, the flow some time after the collapse has sufficient momentum to generate turbulence, but that the necessary triggering mechanism is missing? It is known that some flows can be hydrodynamically stable to infinitesimally small perturbations, but are unstable to finite-size perturbations (as in a pipe flow (Kundu and Cohen (2008)). With respect to the present case, theoretical analysis by Boing et al. (2010) points in this direction. In nature, finite size perturbations are the rule rather than the exception. Also, a clear hint in this direction was given by Shi et al. (2005), who used a local similarity model to simulate the dynamics of the nocturnal boundary layer. By using non-linear analysis they provided support for the potential role of finite scale perturbations in destabilizing the very stable boundary layer, such that sudden regime transitions can occur (their Fig. 4; see also McNider et al. (1995)). Therefore in section 4 the impact of finite size perturbations on the laminarized flow will be examined. Indeed, it will be shown that this type of perturbations may effectively trigger transition to a recovered turbulent flow state i.e. beyond the 'critical' cooling rate. It will also be shown that the velocity profile in this new equilibrium closely corresponds with the profile predicted by the aforementioned analytical analysis. In this way, results of the local similarity model and the DNS are reconciled which leads to the conclusion that $h/L_{ext} = 0.5$ is not 'critical' to the flow.

3. An analytical model

3.1. *Governing equations*

The present work departs from the analytical model introduced by VdW12 with an extension in order to include viscous effects. Here, we will consider the Reynolds averaged equation for momentum and heat for a one-dimensional channel flow which is assumed to be homogeneous in the horizontal direction:

$$\begin{cases} \frac{\partial U}{\partial t} = -\frac{1}{\rho}\frac{\partial P}{\partial x} + \frac{\partial (\tau/\rho)}{\partial z} \\ \frac{\partial T}{\partial t} = -\frac{\partial (H/\rho c_p)}{\partial z} \end{cases} \tag{9}$$

with $U = \bar{u}$ and $T = \bar{T}$ short-hand notations for the horizontally averaged velocity and temperature. Note that we assume a fluid in which humidity has no impact on the buoyancy. The *local* stress τ and the *local* heat flux H are represented by:

$$\begin{cases} \tau = -\rho\overline{u'w'} \\ H/\rho c_p = \overline{w'\theta'}. \end{cases} \tag{10}$$

In VdW12 molecular effects due to viscosity and heat conduction were neglected (representing high Re), except for the fact that an effective roughness length $z_0 = 0.135\nu/u_*$ was chosen in order to mimic hydrodynamically smooth flow as in N05 (Kundu and Cohen (2008)). Below, we summarize the analysis developed in VdW12. In equilibrium, the shape of the profiles does not change in time, therefore, we differentiate (9) with respect to z and consider a steady state.

$$\begin{cases} 0 = \frac{\partial}{\partial t}\left(\frac{\partial U}{\partial z}\right) = \frac{1}{\rho}\frac{\partial^2 \tau}{\partial z^2} \\ 0 = \frac{\partial}{\partial t}\left(\frac{\partial T}{\partial z}\right) = -\frac{1}{\rho c_p}\frac{\partial^2 H}{\partial z^2} \end{cases}, \tag{11}$$

which corresponds to linear flux profiles:

$$\begin{cases} \tau/\tau_0 = u_*^2/u_{*0}^2 = u_*^2/u_{*ext}^2 = 1 - z/h \\ H/H_0 = 1 - z/h \end{cases}. \tag{12}$$

The boundary conditions are given by:

$$\begin{cases} U = 0 \text{ at } z = z_0; \quad \tau = 0 \text{ at } z = h \\ H = H_0 \text{ at } z = z_0; \quad H = 0 \text{ at } z = h \end{cases} \tag{13}$$

Note that the upper boundary condition $H = 0$ is an approximation: in a continuously cooled boundary layer a fixed temperature condition at the top creates a strong top-inversion which acts as a lid on the flow below (see: Derbyshire (1990) and Moene et al. (2010)). The 'steady state' Obukhov length is defined as:

$$L_{ext} = \frac{u_{*ext}^2}{\theta_{*ext}}\frac{T_{ref}}{\kappa g}. \tag{14}$$

By defining:

$$\theta_{*ext} = \frac{1}{u_{*ext}}\frac{-H_0}{\rho c_p} \tag{15}$$

and inserting (12) in (14), we are able to express the steady state local Obukhov length (Λ) in terms of its surface equivalent (with the benefit that the latter can be expressed in external parameters only):

$$\Lambda = \frac{u_*^2}{\theta_*}\frac{T_{ref}}{\kappa g} = L_{ext}\sqrt{1 - z/h}. \tag{16}$$

The log-linear similarity functions relating local fluxes to gradients are adopted as closure assumption to find the equilibrium profiles of U and T:

$$\begin{cases} \frac{\partial U}{\partial z}\frac{\kappa z}{u_*} = 1 + \alpha\frac{z}{\Lambda} \\ \frac{\partial T}{\partial z}\frac{\kappa z}{\theta_*} = 1 + \alpha\frac{z}{\Lambda} \end{cases} \tag{17}$$

which becomes, after inserting (16) in (17) and normalizing with u_{*ext}, θ_{*ext} and h:

$$\begin{cases} \frac{\partial \hat{u}}{\partial \hat{z}} = \frac{\sqrt{1-\hat{z}}}{\kappa\hat{z}} + \frac{\alpha}{\kappa}\frac{h}{L_{ext}} \\ \frac{\partial \hat{\theta}}{\partial \hat{z}} = \frac{\sqrt{1-\hat{z}}}{\kappa\hat{z}} + \frac{\alpha}{\kappa}\frac{h}{L_{ext}} \end{cases} \tag{18}$$

with $\hat{u}$ the scaled velocity, $\hat{\theta}$ the scaled temperature and $\hat{z}$ the normalized height defined as $\hat{z} = z/h$. By integrating the wind profile we obtain the following velocity profile:

$$\hat{u} = \frac{1}{\kappa}\left[2\sqrt{1-\hat{z}} - ln\left(\frac{1+\sqrt{1-\hat{z}}}{1-\sqrt{1-\hat{z}}}\right) + \alpha\hat{z}\frac{h}{L_{ext}}\right]_{\hat{z}_0}^{\hat{z}}. \tag{19}$$

The expression above represents the logarithmic layer and the bulk layer above it. In order to accurately model the velocity profile in the buffer and viscous sublayer an additional correction for viscous effects can be made. Hereto we add viscosity to the turbulent diffusivity and obtain:

$$u_*^2 = \left(\frac{(A\kappa z)^2\frac{\partial u}{\partial z}}{\left(1 + \alpha\frac{z}{\Lambda}\right)^2} + \nu\right)\frac{\partial u}{\partial z}, \tag{20}$$

with A the Van Driest function modifying the traditional mixing length scale (κz) in the buffer layer:

$$A = 1 - \exp\left(-\beta Re_*\right), \tag{21}$$

where $\beta \approx 1/26$ is an empirical constant (Van Driest (1956)). After normalization of (20), $\partial u/\partial z$ should be integrated to obtain the corresponding velocity profile. Unfortunately, the viscous extension makes further analytical integration in (20) intractable, so that we will rely on numerical integration for this case. This extended model is called: local scaling with viscous extension.

3.2. *Comparison with DNS results*

From Figure 3 it appears that for our default case $h/L_{ext} = 0.4$ the turbulent kinetic energy reaches a constant level after $t/t_* = 40$, implying that transient effects have largely disappeared. For this reason we will consider $t/t_* = 40$ as the 'steady state'. In Figure 4 the mean velocity profiles at $t/t_* = 0$ and at $t/t_* = 40$ are compared with the steady state solutions of the analytical local scaling model (and its extension with viscous effects). We observe that the flow is accelerated in its steady state in comparison to its neutral initial state: in stratified conditions vertical turbulent transport is less efficient so that higher shear is needed to maintain the turbulent stress needed to oppose the horizontal pressure gradient. In the analytical formula a value for the free parameter α has to be chosen. Here, we take $\alpha = 7.5$ as a best fit (which will be used in the remainder of the text). We verified that this value gives a good fit for the full range of h/L_{ext} values encountered here. Note that this value is somewhat larger than $\alpha = 5$ typically encountered inn atmospheric studies (Beare (2008), Högström (1996), Howell and Sun (1999), Baas et al. (2006)). Recently, DNS simulation of stratified Ekman layers suggested $\alpha = 5.7$ (Ansorge and Mellado (2014)).

To our knowledge such one-to-one comparison between local similarity and DNS profiles has not been reported previously in literature on atmospheric boundary layers. The correspondence between both models is non-trivial, because local similarity theory was originally derived from atmospheric data which represents much higher Reynolds numbers than the case simulated here.

In VdW12 collapse of turbulence for the present channel flow configuration was explained in terms of the maximum sustainable heat flux theory, using local similarity closure. Therefore, the close correspondence between DNS and local similarity suggests that the same qualitative mechanism is likely to be at play here. This mechanistic aspect of collapse will be elaborated in a follow-up study by the present authors, as here emphasis lies on the revival of turbulent after the collapse stage. The resemblance between both models is in accordance with earlier suggestions by others that DNS may be useful as a complementary tool to study atmospheric-like flows in idealized configurations (Coleman (1999), N05, Flores and Riley (2011); Chung and Matheou (2012); Ansorge and Mellado (2014)).

Note that extension of the model with viscous effects improve the match with DNS in the region close to the surface as compared to the roughness length closure of section 3. At the top of the domain a clear discrepancy between both models is observed. This can be explained by considering the implementation of the upper boundary condition. In both cases the momentum flux is zero at the top of the domain due to the presence of a stress free condition. However, in contrast to the local similarity model which is expressed in horizontal velocity only, DNS has the additional constraint that vertical velocity fluctuations must vanish at the top. This causes an extra suppression of turbulence in this region (which means 'low eddy viscosity'), so that locally higher shear is needed in order to oppose the pressure gradient.

4. Collapse of turbulence: a transient phenomenon

4.1. *Revival of turbulence by finite perturbations*

In VdW12 an analysis similar to Figure 3 was made. As in Figure 3 an initial collapse of turbulence occurred for large values of h/L_{ext}. In contrast, however, the collapse was followed by a recovery at a later stage. The stages of the collapse and recovery were explained as follows: the initial neutrally stratified velocity profile represents a limited amount of momentum. With this momentum and the related shear only a limited amount of heat can be transported downward by the flow: the maximum sustainable heat flux. If the amount of heat extracted at the surface exceeds this maximum the system cannot reach an equilibrium within short term. The stratification near the surface becomes very intense and the turbulence collapses. Later on, the pressure gradient accelerates the flow. With increasing shear also the heat transport capacity of the flow rapidly increases, until finally enough kinetic energy is built up to break through the stratification.

In view of the correspondence between the local-similarity model and DNS in Figure 4, a similar mechanism is likely to occur here. As such, it seems reasonable to assume that sufficient kinetic energy has been built up after a certain period of time to enable recovery. Then, if regeneration does not occur spontaneously, this could be due to the fact that perturbations in the idealistic model environment are too weak to trigger instability. In nature however, finite-size perturbations of various origin (topography, heterogeneity) are realistic features and will commonly occur. So the question is: how to kick the flow with a 'realistic' finite perturbation?

In another context, an inspiring view was given by Cekli et al. (2010) regarding wind tunnel turbulence. They showed that resonance enhancement of turbulence intensity could be obtained by perturbing the flow with a frequency equal to the eddy-turnover rate of the energy containing eddies (stirring turbulence with turbulence). Here, our mere goal is to show that it is the lack of triggering rather than the lack of shear that prevents a spontaneous recovery of turbulence in idealized DNS studies as in N05. As such, we adopt a practical approach inspired by the aforementioned wind tunnel study. To this end, we will use the turbulence structures in the (surviving) $h/L_{ext} = 0.4$ case as to trigger turbulence in the collapsed $h/L_{ext} = 0.6$ case. Mathematically, we define the perturbed velocity vector field u' as the instantaneous field u at $t_* = 25$ minus its horizontally averaged field $< u >$. The perturbed velocity vector field is expressed as:

$$u'_{h/L=0.4} = u_{h/L=0.4} - < u_{h/L=0.4} > . \tag{22}$$

We expect that the dominant modes in the $h/L_{ext} = 0.4$ turbulence will be effective trigger modes at $h/L_{ext} = 0.6$ (although the integral length scale will be somewhat smaller in the latter). In order to keep the perturbation limited in magnitude, we divide the intensity of the trigger turbulence by 10. This 3D perturbation field trigger is then applied to the velocity components and likewise to temperature. The perturbed velocity field formally reads:

$$u_{h/L=0.6}(t_* > 15) = u_{h/L=0.6}(t_* = 15) + \frac{1}{10} u'_{h/L=0.4}(t_* = 25) \tag{23}$$

Next, it should be realized that the perturbation is free to 'die out'. In case the flow would be intrinsically laminar this perturbation would still die out. On the other hand, in case the flow is potentially turbulent, a recovery will occur. Indeed, the latter appears to be

the case (Figure 5). Hence, we may conclude that the laminar state at $t/t_* = 15$ was ready to become turbulent. Again, our primary goal is merely to show that some kind of perturbations indeed *can* trigger a flow transition, so that the lack of triggering is the cause of persistent collapse rather than the absence of sufficient kinetic energy. Of course, many alternative (and formal) perturbation methods could be applied. However, an in-depth analysis of various potential perturbation techniques is beyond the scope of the present work.

In Figure 6 the time trace of the turbulence kinetic energy (a) and turbulent stress (b) are shown. The revival of turbulence after the 'kick' is clearly visible in both graphs. The strong 'overshoot' in turbulent kinetic energy results from the rapid conversion from mean kinetic energy to its turbulent counter part (see discussion below). Note that in absence of triggering, the default case (dashed), reveals a gradual increase in turbulent kinetic energy. However, this increase is likely due to non-turbulent variance in the (horizontal) velocity components, for example due to meandering of the flow, as it is absence in the evolution of turbulent stress (Figure 6 (b)).

In Figure 7 the corresponding mean velocity profiles before and after the triggering are depicted. Also the equilibrium profile, predicted by the analytical model, is given (red line). The dashed line represents the state just before triggering. The flow has large momentum compared to the initial neutral state (e.g. Figure 4) as a result of the acceleration after the collapse. After the sudden transition to turbulence, mean kinetic energy is converted into turbulent kinetic energy and significant Reynolds stresses slow down the flow and it evolves towards its equilibrium state (black line). The simulated equilibrium state is in close agreement with the analytical prediction of the $h/L_{ext} = 0.6$ steady state.

Next, sensitivity of the recovery to the timing and magnitude of the triggering was investigated. Interestingly, when the same perturbation was added at an earlier stage ($t/t* = 10$ instead of 15) it did not lead to a recovery and the added perturbation rapidly dissipated into the laminar background flow. Apparently, at this stage the generated momentum was still insufficient to generate turbulence under those strongly stratified conditions. Another case was investigated, where the timing of the perturbation ($t_* = 15$) was kept constant, but the magnitude of the perturbation was lowered by a factor of $2/3$. Again, the perturbation rapidly dissipated. This indicates that the perturbation field requires certain intensity in order to trigger a full transition to turbulence. Both permutations stress that the perturbation itself is of importance. A full sensitivity analysis, however, is beyond the scope of the present work. Here, the aim is to provide evidence that essentially the collapse of turbulence in a pressure driven channel flow is a transient phenomenon and that such thing as a 'critical' cooling rate does not exist for such configuration.

4.2. *Influence of the initial conditions*

In section 1 it was argued that, according to the maximum sustainable heat flux hypothesis, a flow with sufficient initial momentum (or with sufficient *shear capacity*: $U/U_{min} > 1$ (Van Hooijdonk et al. (2014)), also Figure 1) has enough heat transport capacity and therefore should be able to remain turbulent at 'supercritical' cooling rates. In order to investigate this, we performed an experiment where the initial neutral field is replaced by the analytical solution for $h/L_{ext} = 0.6$ in its equilibrium state (Figure 8). Because of stability this case has larger momentum than the default initial case. Next, turbulent fluctuations of the steady state $h/L_{ext} = 0.4$ field are added, such that the initial field has turbulent properties. The total initial field is visualized by Figure 9 (a). In mathematical terms the initial field hence reads:

$$u_{initial} = u_{ana}(h/L = 0.6) + u'_{h/L=0.4} \tag{24}$$

The simulation is run for $t = 25t_*$, while applying continuous 'supercritical' cooling ($h/L_{ext} = 0.6$) at the surface. As anticipated, the case remains turbulent and no collapse occurs, even though strong, 'supercritical' cooling was applied during the full period. This is also clear from Figure 10 (a) which shows the domain integrated kinetic energy as a function of time. Finally, the simulated equilibrium profile remains close to the anticipated profile (Figure 10 (b)), apart from the discrepancy near the top of the channel, which again is related to the boundary layer issue at the top, discussed in section 3.

5. Discussion

5.1. *Collapse of turbulence and relation to the turbulent kinetic energy budget*

The purpose of this section is to show that the existence of turbulence at 'supercritical' cooling rates is compatible with turbulent kinetic energy budget analysis. In the present framework (VdW12, Van de Wiel et al. (2007)), a regime transition (temporary collapse of turbulence) is predicted when the flow just after the onset of cooling is unable to support the heat loss at the surface (Figure 1). It is shown that it is the interplay between the flow and the boundary conditions enables a positive feedback which may lead to a sudden intensification of the density stratification near the surface. Then, eventually, length scales in the flow become so small that continuous turbulence cannot be sustained (at least temporarily).

From a different point of view, traditionally, the transition between the continuous turbulent regime and the very stable regime is often discussed in terms of turbulent kinetic energy budget analysis (e.g. Wyngaard (2008)). The idea is that, in order to maintain steady turbulence of significant magnitude the buoyancy destruction term should not exceed the shear production term. In other words the flux Richardson number Rf should be smaller than one (see below). Recently, however, this traditional view has been opposed. It has been shown that a different regime may appear but that weak levels of turbulence may still be present at larger values of the Rf and that the concept of critical Richardson number no longer exists (Galperin et al. (2007), Mauritsen and Svensson (2007), Zilitinkevich et al. (2007), Rodrigo and Anderson (2013), Grachev et al. (2013) and Zilitinkevich et al. (2008)).

Here, this issue at large Rf-values is not debated. It is namely important to realize that regime transition according to the concept in Figure 1 occurs when Ri is only $O(0.1)$, see: VdW12. As the turbulent Prandtl number is still close to one at weak stability, this implies that a transition is predicted for $Rf = O(0.1)$. It is only after this transition where the recent discussion on the existence of turbulence/no turbulence at $Rf = O(1)$ sets in, which is not discussed here. The aforementioned hypothesis just states that the emergence of a completely different atmospheric regime is to be expected when the positive feedback of Figure 1 sets in. Though, in the DNS channel flow this transition leads to a temporary laminarisation, in reality this may coincide with a regime with some reminiscent, weak or intermittent turbulence (Sun et al. (2012); Van de Wiel et al. (2003); Ansorge and Mellado (2014)). But, even

in the present study is has been shown that the positive feedback is counteracted by a flow acceleration, which enables a recovery of turbulence in the long-term.
Here, nevertheless a theoretical turbulent kinetic energy budget analysis is presented, in order to put our result in perspective of the discussion in Wyngaard (2008) and N05. It will be shown, that in equilibrium flow Rf remains finite (and smaller than 1) even if h/L_{ext} goes to infinity. This counter-intuitive result is due to the flow acceleration which causes the shear production term to become proportional to h/L_{ext}, thus keeping Rf finite.

5.2. *Equilibrium state for $h/L_{ext} \to \infty$*

In section 3, it has been shown that the analytical expression (19) closely corresponds to the steady state velocity profile obtained with DNS. Next, we will use the analytical model to investigate what will happen to the domain-averaged shear production and buoyancy destruction in case h/L_{ext} goes to infinity. In other words: what happens to the domain averaged flux Richardson number when $h/L_{ext} \to +\infty$?
As point of departure the turbulent kinetic energy equation is considered:

$$\frac{\partial e}{\partial t} = -\overline{u'w'}\frac{\partial \overline{u}}{\partial z} + \frac{g}{T_{ref}}\overline{w'\theta'} - \frac{\partial \overline{w'e}}{\partial z} - \frac{1}{\rho}\frac{\partial \overline{w'p'}}{\partial z} - \epsilon. \tag{25}$$

The time evolution of the turbulence depends on the production of turbulence by wind shear, the destruction of turbulence by buoyancy and the dissipation of turbulence. The turbulent transport and the pressure correlation terms only act to redistribute the turbulent kinetic energy and pressure fluctuations vertically. The flux Richardson number Rf measures the ratio between buoyancy destruction and production of turbulence. In order to globally characterize the flow, we will consider the vertically integrated domain averaged flux Richardson number $\langle Rf \rangle$:

$$\langle Rf \rangle = \frac{\int_{z_0}^{h} \frac{g}{T_{ref}}\overline{w'\theta'}dz}{\int_{z_0}^{h} \overline{u'w'}\frac{\partial \overline{u}}{\partial z}dz}. \tag{26}$$

Next we use the fact that the *local* stress values $-\overline{u'w'}$ (also denoted here as u_*^2) is related to the surface values u_{*ext}^2 via (12):

$$\begin{cases} u_*^2 = u_{*ext}^2(1 - z/h) \\ u_*\theta_* = u_{*ext}\theta_{*ext}(1 - z/h), \end{cases} \tag{27}$$

and we express the flux Richardson number in terms of scaled parameters like $\hat{z} = z/h$ and $\hat{u} = \overline{u}/u_{*0}$:

$$\langle Rf \rangle = \frac{\int_{\hat{z}_0}^{1} \frac{g}{T_{ref}}\frac{\theta_{*ext}h}{u_{*ext}^2}\hat{u}_*\hat{\theta}_* d\hat{z}}{\int_{\hat{z}_0}^{1} \hat{u}_*^2\frac{\partial \hat{u}}{\partial \hat{z}}d\hat{z}} = \frac{\frac{h}{L_{ext}}\int_{\hat{z}_0}^{1}(1-\hat{z})d\hat{z}}{\kappa\int_{\hat{z}_0}^{1}(1-\hat{z})\frac{\partial \hat{u}}{\partial \hat{z}}d\hat{z}}. \tag{28}$$

Elaboration of the numerator learns that the buoyancy destruction amounts is $(1/2)h/L_{ext}$ using ($\hat{z}_0 \ll 1$). The denominator (shear production) becomes:

$$\kappa\int_{\hat{z}_0}^{1}(1-\hat{z})\frac{\partial \hat{u}}{\partial \hat{z}}d\hat{z} = \kappa\left[(1-\hat{z})\hat{u}\right]_{\hat{z}_0}^{1} + \kappa\int_{\hat{z}_0}^{1}\hat{u}d\hat{z} = \kappa\int_{\hat{z}_0}^{1}\hat{u}d\hat{z}, \tag{29}$$

where we used the fact that the momentum flux at the top and the velocity at the surface vanishes. As such the total shear production is determined by the integrated velocity profile given by (19). Before using this rather complicated expression directly, we will first approximate (19) by using the traditional log-linear velocity profile instead of its exact local counterpart. The traditional log-linear velocity profile is written as:

$$\hat{u} = \frac{1}{\kappa}\left[ln\left(\frac{\hat{z}}{\hat{z}_0}\right) + \alpha\hat{z}\frac{h}{L_{ext}}\right]. \tag{30}$$

Note that this expression (30) is merely an asymptotic case of the general formula (19) for $z \ll h$ (VdW12). Then the integral in (29), i.e. the denominator of (28), can be written as:

$$\begin{aligned} \kappa\int_{\hat{z}_0}^{1}\hat{u}d\hat{z} &= \int_{\hat{z}_0}^{1} ln\left(\frac{\hat{z}}{\hat{z}_0}\right) + \alpha\hat{z}\frac{h}{L_{ext}}d\hat{z} \\ &= \left[\hat{z}ln\left(\frac{\hat{z}}{\hat{z}_0}\right) - \hat{z} + \alpha\frac{h}{L_{ext}}\frac{1}{2}\hat{z}^2\right]_{z_0}^{1} \\ &= ln\left(\frac{1}{\hat{z}_0}\right) - 1 + \alpha\frac{1}{2}\frac{h}{L_{ext}} \\ &\quad + \hat{z}_0 - \hat{z}_0^2\alpha\frac{1}{2}\frac{h}{L_{ext}}. \end{aligned} \tag{31}$$

By assuming that the last two terms are negligible ($z_0 \ll 1$), we obtain:

$$\langle Rf \rangle \approx \frac{\frac{1}{2}\frac{h}{L_{ext}}}{\alpha\frac{1}{2}\frac{h}{L_{ext}} + ln(\frac{h}{z_0}) - 1}. \tag{32}$$

For the general case, the same reasoning applies: the h/L_{ext} term in eq. (19) will start to dominate for $h/L_{ext} \to \infty$ so that $\langle Rf \rangle \to 1/\alpha$. Hence Rf remains finite (and inferior to 1). The physical interpretation is as follows: as the imposed surface cooling increases, vertical transport is less and less efficient. In steady state, however, the (surface) stress is by definition determined by the horizontal pressure gradient which it has to balance. As the effective 'eddy viscosity' is decreasing with increasing surface cooling the shear needs to increase accordingly. Eventually the proportionality of the turbulent kinetic energy shear destruction with h/L_{ext} compensates the increasing buoyancy destruction such that the ratio remains constant.
This finding supports Nieuwstadt's conclusion using the simplified analytical approach: from a turbulent kinetic energy perspective, steady state turbulence appears sustainable in the limit $h/L_{ext} \to +\infty$. Apart from this discussion on TKE, it would be interesting to analyse this configuration using the concept of total turbulent energy as suggested by Zilitinkevich et al. (2008).

Finally, we comment briefly on a erroneous interpretation on N05 results by Wyngaard (2008). In his analysis (pp. 285,291) he uses the assumption that Rf cannot exceed 1 if the turbulence is to be sustained. Next, however, for simplicity reasons, a Moody chart is used in order to relate depth average wind speed - to be inserted in (29) - to the pressure gradient. But as the Moody chart represent neutrally stratified flow only, it will not represent the fact that shear and hence, averaged velocity, increases with stability as in (30). In our case the 'Moody approach' would imply to ignore the $\alpha h/L_{ext}$ part in the integral. As a consequence this leads to the erroneous conclusion that the constraint $\langle Rf \rangle < 1$ translates in an upper value (critical value) for h/L_{ext}.
To summarise: from a TKE-perspective Nieuwstadt's suggestion that analysis on flow energetics cannot substantiate a critical h/L_{ext} is correct.Through on the short-term turbulence may collapse due to the fact that the initial momentum and hence the maximum sustainable heat flux is limited, on long-term the system is able to reach a turbulent steady state again. Yet, the direct numerical simulations reveal a clear flow transition for $h/L_{ext} \approx 0.5$. In section 4, we showed that the solution to this paradox lies in the numerical simulations themselves.

5.3. Generality of the results and impact of the boundary condition

In our idealistic set up surface cooling is imposed instantaneously for $t/t_* > 0$. In reality the transition to nocturnal conditions rather sets in on a finite time-scale τ. Theoretical analysis (VdW12) has shown that a temporary collapse of turbulence is possible due to the fact that the flow acceleration time scale is much larger than the time scale at which the change in surface condition is being diffused (upward mixing of cold air). It is therefore expected that, when surface cooling would be imposed more gradually, this largely would moderate the chance of collapse as the shear generation has more time to adapt to the new surface boundary condition. In future, this relevant aspect should be studied in more detail.
In the present study a modest frictional Reynolds number of 360 is used in the analysis in order to study N05-case. From Flores and Riley (2011) it is known that an increase in Reynolds number leads to a larger value of the 'critical' h/L_{ext}, i.e. in a transient sense. For example their $Re_* = 560$ showed that $h/L_{ext_{crit}} = 0.82$ instead of 0.5. With respect to atmospheric applications it would be interesting if this transient, 'critical' h/L_{ext} reaches some of asymptotic value for $Re_* \to +\infty$.

Note that strong caution has to be taken when inter-comparing results with respect to laminarization when different model configurations are used. Similar as in N05, Jimenez and Cuxart (2005), Flores and Riley (2011) and Deusebio et al. (2011) stratification is created in the present study by imposing a fixed surface heat flux such that the flow is characterized by h/L_{ext} as the external parameter.
In other studies like e.g. Armenio and Sarkar (2002) and Gracía-Villalba and Del Álamo (2011), stratification is imposed by setting a constant temperature difference. In that case the flow is characterized by some form of a bulk Richardson number instead of h/L_{ext}. Though both configurations may lead to similar velocity and temperature profiles their 'resistance to laminarization' can be completely different. In atmospheric terms: a given temperature inversion and wind profile could endure a collapse event over insulating fresh snow (which acts like a flux boundary condition driven by net radiative cooling), whereas the same mean temperature and wind profile could allow survival of turbulence over melting snow (which acts like a temperature boundary condition). As such the dynamical system response cannot be viewed separately from its boundary condition. This aspect as well as more concrete atmospheric implications are discussed in detail in VdW12.
Finally, it is stressed that the present simplified set up in the form of a flux-driven channel flow largely limits the dynamical richness as compared to real atmospheric boundary layers. In particular no evidence of globally intermittent turbulence was found here, though this characteristic is frequently encountered in strongly stratified nocturnal boundary layers (e.g. Van de Wiel et al. (2003); Sun et al. (2004)). Also, aforementioned studies on similar regime transitions with local similarity modeling by VDW12 and Shi et al. (2005), did not show evidence of any (quasi) 'cyclic' breakdown of turbulence. Ansorge and Mellado (2014), on the other hand clearly demonstrated that large spatial intermittency can be generated by internal system dynamics when Coriolis effects are included in Direct Numerical Simulations. In Large-Eddy Simulations by Zhou and Chow (2011) inclusion of Coriolis effects enabled formation of Low-Level Jets, which intermittently induced instabilities to occur due to the presence of an inflection point in the velocity profile. Recently, it has also been demonstrated that velocity inflection points at the top of large canopies may generate intermittent behaviour of turbulence in strongly stratified flows (Boing et al. (2010); see also: Patton et al. (2011)). Note that the dynamical implications of velocity inflection points in terms of hydrodynamic stability cannot be diagnosed as such in simple 'eddy viscosity' models as in VDW12 and Shi et al. (2005). Apart from those aspects, also surface heterogeneity in combination with local topography may introduce new dynamics as compared to homogeneous flows (McNider and Pielke (1984)). A clear observational example is given by the study of Acevedo et al. (2003), where on a relatively small horizontal separation distance both coupled and decoupled boundary layers occurred simultaneously, with their actual state depending on the local surface elevation and local wind regime.

6. Conclusion

In this work, a theoretical cooled channel flow configuration is used in order to make a one-to-one comparison between an 'atmospheric' local similarity model and a direct numerical simulation 'model', which actually resolves turbulent motions down to the Kolmogorov

scale. Both methodologies lead to steady state velocity profiles which are remarkably similar (likewise for temperature: not shown). Although only a limited number of (moderate Re_*) cases have been studied, in our opinion this indicates that, potentially, DNS can potentially be a useful complementary tool to study 'atmospheric' stable boundary layer dynamics in addition to other models like LES and Reynolds-averaged modelling simulation (RANS) models; which represent high Reynolds number flows.

Next, the process of flow laminarization in response to enhanced surface cooling (h/L_{ext}) has been studied. Though earlier studies coined the existence of a critical cooling rate ($h/L_{ext} \sim 0.5$; or $h/L_{ext} \sim 1.23$ when the Von Kármán constant is excluded in the definition), it is shown here that the cooling rate itself is not critical for the turbulence to survive. In fact when sufficient initial momentum is imposed cooling rates beyond $h/L_{ext} \sim 0.5$ can be sustained. Likewise, it has been shown that a collapse for $h/L_{ext} \sim 0.5$ is only temporary due to the fact that such collapse is followed by flow acceleration. When sufficient shear has been built up, turbulence is regenerated provided that finite perturbations of sufficient magnitude are present in the flow (which in outdoor, geophysical flows is generally the case). As such, the present analysis suggests that collapse of turbulence in the evening boundary layer is mostly a transient phenomenon.

Acknowledgement

This work as been supported by a VIDI Grant (1001425) from the Dutch National Science Foundation (NWO), which is gratefully acknowledged. The authors also would like to thank Prof. John Wyngaard for his suggestion to analyse the turbulent kinetic energy budget.

References

Acevedo OC, Fitzjarrald DR. 2003. In the core of the night-Effects of intermittent mixing on a horizontally heterogeneous surface. *Bound.-Layer Meteor.*. 106:1-33.

Acevedo OC, Costa FD and Degrazia GA. 2012. The Coupling State of an Idealized Stable Boundary Layer. *Bound.-Layer Meteor.*. 145:211-228.

Rodrigo JS and Anderson PS. 2013. Investigation of the Stable Atmospheric Boundary Layer at Halley Antarctica. *Bound.-Layer Meteor.*. 148:517-539.

Armenio V and Sarkar S. 2002. An investigation of stably stratified turbulent channel flow using large-eddy simulation. *J. Fluid Mech.*. 459:1-42.

Ansorge C and Mellado JP. 2014. Global intermittency and collapsing turbulence in a stratified planetary boundary layer. *Bound.-Layer Meteor.*. 153:89-116.

Baas P, Steeneveld GJ, Van de Wiel BHJ and Holtslag AAM. 2006. Exploring self Correlation in flux-gradient relationships for stably stratified conditions. *J. Atmos Sci*. 63:3045-3054.

Basu S, Porté-Agel F, Foufoula-Georgiou E, Vinuesa JF and Pahlow M. 2006. Revisiting the local scaling hypothesis in stably stratified atmospheric boundary layer turbulence: An integration of the field and laboratory measurements with large-eddy simulations. *Bound.-Layer Meteor.*. 119:473-500.

Beare RJ. 2008. The role of shear in the morning transition boundary layer. *Bound.-Layer Meteor.*. 129:395-410.

Boing S, Jonker HJJ, Van de Wiel BJH and Moene AF. 2010. Intermittent Turbulence in Stratified Flow over a Canopy. *19th Symposium on Boundary Layers and Turbulence Annual Meeting of the European Meteorological Society*

Businger JA. 1973. Turbulent transfer in the atmospheric surface layer*Workshop on Micrometeorology, Amer. Meteor. Soc.*. Boston; pp 67-100.

Cekli HE, Tipton C and van de Water W. 2010. Resonant Enhancement of Turbulent Energy Dissipation. *Phys. Review Lett.*. 105:044503.

Chung D and Chung G . 2012. Direct numerical simulation of stationary homogeneous stratified sheared turbulence. *J. Fluid. Mech.*. 696:434-467.

Coleman GN. 1999. Similarity Statistics from a Direct Numerical Simulation of the Neutrally Stratified Planetary Boundary Layer. *J. Atmos Sci*. 56:891-900.

Costa FD, Acevedo OC, Mombach JCM, Degrazia GA. 2011. A Simplified Model for Intermittent Turbulence in the Nocturnal Boundary Layer. *Bound.-Layer Meteor.*. 68:1714-1729.

Cuxart J, Yagüe C, Morales G, Terredellas E, Orbe J, Calvo J, Fernandez A, Soler MR, Infante C, Buenestado P, Espinalt A, Joergensen HE, Rees JM, Vilà J, Redondo JM, Cantalapiedra IR and Conangla L. 2000. Stable atmospheric boundary-layer experiment in Spain (SABLES 98): a report. *Bound.-Layer Meteor.*. 96:337-370.

Cuxart J and Jimenez MA. 2007. Mixing processes in a nocturnal low-level jet: An LES study. *J. Atmos. Sci.*. 64:1666-1679.

Delage Y, Barlett PA and McCaughey JH. 2002. Study of 'soft night-time surface layer decoupling over forest canopies in a land-surface model. *Bound.-Layer Meteor*. 103:253-276.

Derbyshire SG. 1990. Nieuwstadt's stable boundary layer revisited. *Quart. J. Roy. Meteor. Soc.*. 116:127-158.

Deusebio E, Schlatter P, Brethouwer G and Lindborg E. 2011. Direct numerical simulations of stratified open channel flows. *J. Phys.: Conf. Ser.*. 318:022009

Edwards EJM. 2009. Radiative Processes in the Stable Boundary Layer:Part II. The Development of the Nocturnal Boundary Layer. *Bound.-Layer Meteor*. 131:127-146.

Flores O and Riley JJ. 2011. Analysis of turbulence collapse in the stably stratified surface layer using direct numerical simulation. *Bound.-Layer Meteor*. 139:241-259.

Galperin B, Sukoriansky S, and Anderson PS. 2007. On the critical Richardson number in stably stratified turbulence. *Atmos. Sci. Lett.*. 8:5-69.

Gracía-Villalba M and Del Álamo JC. 2011. Turbulence modification by stable stratification in channel flow. *Phys. Fluids*. 23:045104.

Grachev AA, Fairall CW, Persson POG, Andreas EL, and Guest PS. 2005. Stable boundary layer dcaling regimes: the SHABA data. *Bound.-Layer Meteor*. 116:201-235.

Grachev AA, Andreas EL, Fairall CW, Guest PS and Persson POG. 2013. The Critical Richardson Number and Limits of Applicability of Local Similarity Theory in the Stable Boundary Layer. *Bound.-Layer Meteor.*. 147:51-82.

Hoch SW and Calanca P. 2007. Year-Round Observation of Longwave Radiative Flux Divergence in Greenland. *J. Appl. Meteor. Climatol.*. 46:1469-1479.

Högström U. 1996. Review of some basic characteristics of the atmospheric surface layer. *Bound.-Layer Meteor*. 78:215-246.

Holtslag AMM, Svensson G, Baas P, Basu S, Beare B, Beljaars ACM, Bosveld FC, Cuxart J, Lindvall J, Steeneveld GJ, Tjernström and Van de Wiel BJH. 2013. Stable atmospheric boundary layers and diurnal cycles-challenges for weather and climate models. *Bull. Amer. Meteor. Soc.*. Early Online Releases.

Howell J and Sun J. 1999. Large-eddy simulations of the stable boundary layer using the standard Kolmogorov theory: range of applicability. *Bound.-Layer Meteor*. 115:241-261.

Huang J,Bou-Zeid E. 2013. Turbulence and Vertical Fluxes in the Stable Atmospheric Boundary Layer. Part I: A Large-Eddy Simulation Study. *J. Atmos. Sci.*. 70:1513-1527.

Jimenez MA and Cuxart J. 2005. Surface layer fluxes in stable conditions. *Bound.-Layer Meteor*. 90:495-520.

Kundu PK, Cohen IM. 2008. *Fluid Mechanics*. Academic Press;pp 872.

Łobocki L. 2013. Analysis of Vertical Turbulent Heat Flux Limit in Stable Conditions with a Local Equilibrium, Turbulence Closure Model. *Bound.-Layer Meteor.*. 148:541-555.

Mahrt L. 1998. Flux Sampling errors for aircraft and towers. *J. Atmos. Oceanic Technol.*. 15:416-429.

Mahrt L. 2011. The near-calm stable boundary layer. *Bound.-Layer Meteor.*. 140:343-360.

Mahrt L. 2014. Stably stratified atmospheric boundary layers. *Annual rev. of Fluid Mech.*. 74:389-396.

Malhi YS. 1995. The significance of the diurnal solutions for heat fluxes measured by the temperature fluctuation method in stable conditions. *Bound.-Layer Meteor.*. 74:389-396.

Mauritsen T and Svensson G. 2007. Observations of stably stratified shear-driven atmospheric turbulence at low and high Richardson numbers. *J. Atmos. Sci.*. 64:645-655.

McNider RT and Pielke RA. 1984. Numerical simulation of slope and mountain flows. *J. Climate Appl. Meteor.*. 23:1441-1453.

McNider RT, England DE, Friedman MJ and Shi X. 1995. Predictability of the Stable Atmospheric Boundary Layer. *J. Atmos. Sci.*. 52:1602-1614.

Moene AF. 2003. Swirling pipe flow with axial strain: experiment and large eddy simulation. *PhD thesis*. Technical University Eindhoven. ISBN 90-386-1695-3, 237 pp.

Moene AF, Van de Wiel BJH and Jonker HJJ. 2010. Local similarity profiles from direct numerical simulation. *19th Symp. on Boundary Layers and Turbulence*

Nieuwstadt FTM. 2005. Direct numerical simulation of stable channel flow at large stability. *Bound.-Layer Meteor.*. 116: 277-299.

Patton EG, Horst TW, Sullivan PP, Lenschow DH, Oncley SP, Brown WOJ, Burns SP, Guenther AB, Held A, Karl T, Mayor SD, Rizzo LV, Spuler SM, Sun J,Turnipseed AA, Allwine EJ, Edburg SL, Lamb BK, Avissar R, Calhoun RJ, Kleissl J, Massman WJ, Paw U KT U, Weil JC. 2011. The canopy horizontal array turbulence study. *Bull. Amer. Meteor. Soc.*. 92:593-611.

Poulos GS, Blumen W, Fritts DC, Lundquist JK, Sun J, Burns SP, Nappo C,Banta R, Newsom R, Cuxard J, Terradellas E, Balsley B and Jensen M. 2002. CASES-99: A Comprehensive Investigation of the Stable Nocturnal Boundary Layer. *Bull. Amer. Meteor. Soc.*. 83:555-581.

Shi X, McNider RT, England DE, Friedman MJ, Lapenta W and Norris WB. 2005. On the behavior of the stable boundary layer and role of initial conditions. *Pure Appl. Geophys.*. 162:18111829.

Sorbjan Z. 2006. Local structure of turbulence in stably stratified boundary layer. *J. Atmos. Sci.*. 63:1526-1537.

Sun J, Mahrt L, Burns SP, Banta RM, Newsom RK, Coulter R, Frasier S, Ince T, Nappo C, Balsley BB, Jensen M, Mahrt L, Miller D and Skelly B. 2004. Atmospheric disturbances that generate intermittent turbulence in nocturnal boundary layers. *Bound.-Layer Meteor.*. 100:255-279.

Sun J, Mahrt L, Banta RM, Pichugina YL. 2012. Turbulence Regimes and Turbulence Intermittency in the Stable Boundary Layer during CASES-99. *J. Atmos. Sci.*. 69:338-351.

Taylor PA. 1971. Log-linear velocity profile in stable conditions. *Quart. J. Roy. Meteor. Soc.*. 97:326-329.

van Driest ER. 1956. On turbulent flow near a wall. *J. Aeronaut. Sci. 23*. 11:1007-1011.

Van Hooijdonk IGS, Donda JMM, Clercx JH, Bosveld FC and Van de Wiel BJH. 2014. Shear capacity as prognostic for nocturnal boundary layer regimes. *J. Atmos. Sci.*. Early Online Releases, doi: 10.1175/JAS-D-14-0140.1.

Van de Wiel BJH, Ronda RJ Moene AF, De Bruin HAR and Holtslag AAM. 2002. Intermittent turbulence and oscillations in the stable boundary layer. Part I: A bulk model. *J. Atmos. Sci.*. 59:942-958.

Van de Wiel BJH, Moene AF, Hartogensis OK, De Bruin HAR and Holtslag AAM. 2003. Intermittent turbulence in the stable boundary layer over land. Part III: A classification for observations during CASES-99. *J. Atmos. Sci.*. 60:2509-2522.

Van de Wiel BJH, Steeneveld GJ, Hartogensis OK and Holtslag AAM. 2007. Predicting the collapse of turbulence in stably stratified boundary layers. *Flow Turbul. Combust.*. 79:251-274.

Van de Wiel BJH, Moene AF, Jonker HJJ and Holtslag AAM. 2012. The Cessation of Continuous Turbulence as Precursor of the Very Stable Nocturnal Boundary Layer. *J. Atmos. Sci.*. 69:3097-3115.

Wyngaard JC. 2008. *Turbulence in the Atmosphere*. Cambridge University Press:New York;pp 291.

Zilitinkevich SS, Elperin T, Kleeorin N and Rogachevskii I. 2007. Energy- and flux-budget (EFB) turbulence closure model for stably stratified flows. Part I: Steady state, homogeneous regimes. *Bound.-Layer Meteor.*. 125:167-191.

Zilitinkevich SST, Elperin T, Kleeorin N, Rogachevskii I, Esau I, Mauritsen T, Miles MW. 2008. Turbulent energetics in stably stratified geophysical flows: Strong and weak mixing regimes. *Quart. J. Roy. Meteor. Soc.*. 134:793-799.

Zilitinkevich SST, Elperin T, Kleeorin N, Rogachevskii I, Esau I. 2013. A Hierarchy of Energy- and Flux-Budget (EFB) Turbulence Closure Models for Stably-Stratified Geophysical Flows. *Bound.-Layer Meteor.*. 146:341-373.

Zhou B and Chow K. 2011. Large-eddy simulation of the stable boundary layer with explicit filtering and reconstruction turbulence modeling. *J. Atmos. Sci.*. 68:2142-2155.

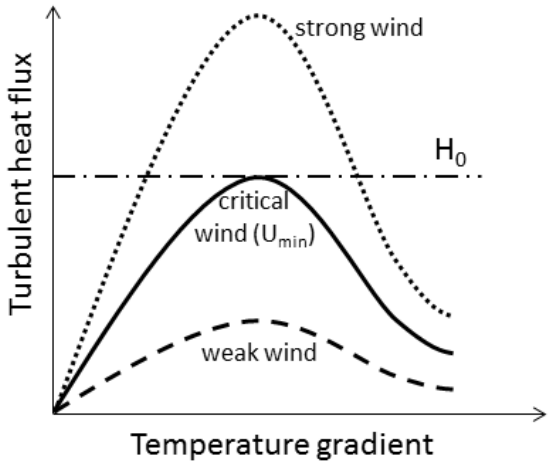

Figure 1. Schematic picture depicting the typical dependence of the atmospheric turbulent heat flux on the near surface temperature gradient in stably stratified conditions(here, plotted positive for convenience). The curve represent dependencies for weak wind (dashed line), strong wind (dotted line) and critical wind condition (continuous line).

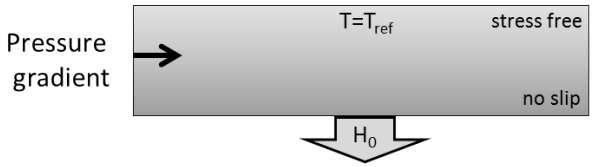

Figure 2. Schematic picture of our set-up considering a horizontally homogeneous channel flow. Decreasing temperature is indicated by an increasing grey-scale.

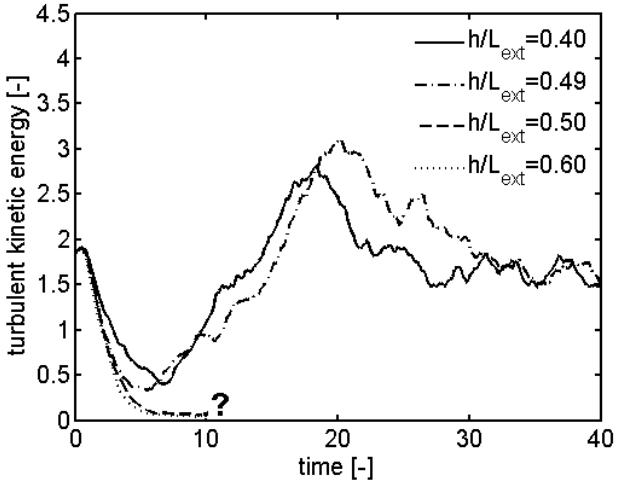

Figure 3. Temporal evolution of scaled turbulence kinetic energy in a stably stratified channel flow. The cases represent different cooling rates, in dimensionless form represented by h/L_{ext} values as indicated.

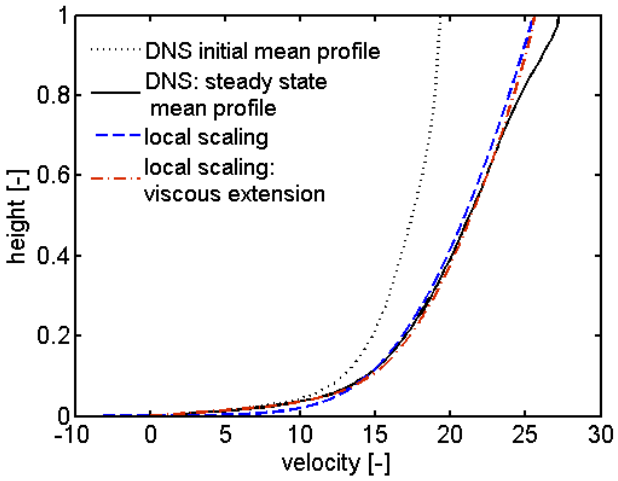

Figure 4. Comparison of the steady state mean velocity profile for the case $h/L_{ext} = 0.4$ (continuous black line) with the analytical solution calculated following the z_0 concept (dashed blue line) and the analytical solution adding the viscous effect (dotted red line). The initial neutral velocity profile is presented by the dash-dotted black line.

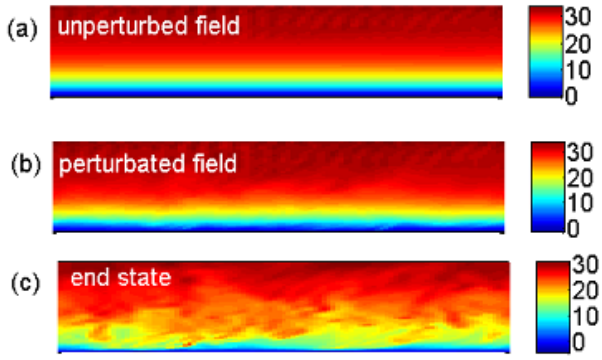

Figure 5. Vertical cross-section of the velocity field magnitude prior and after perturbation of the mean velocity field:(a) undisturbed, laminar field at $t/t_* = 15$ for the collapse $h/L_{ext} = 0.6$ case. (b) Visualisation of the perturbed field (Eq. 23) one time-step after $t/t_* = 15$. (c) field at $t/t_* = 40$ ('end state'). Colours indicate the dimensionless magnitude of the velocity.

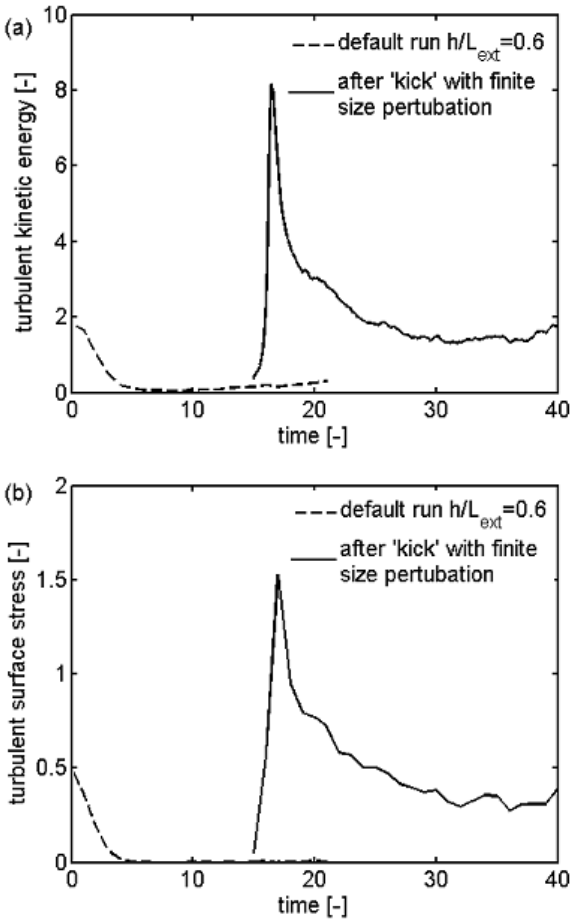

Figure 6. Temporal evolution of turbulent kinetic energy (a) and the turbulent surface stress (b) both for 'supercritical' $h/L_{ext} = 0.6$ case with neutral initial condition. Dashed line indicates evolution of the default run showing a rapid collapse of turbulence. Continuous line represents simulation after adding finite perturbations on the laminarized field at $t/t_* = 15$.

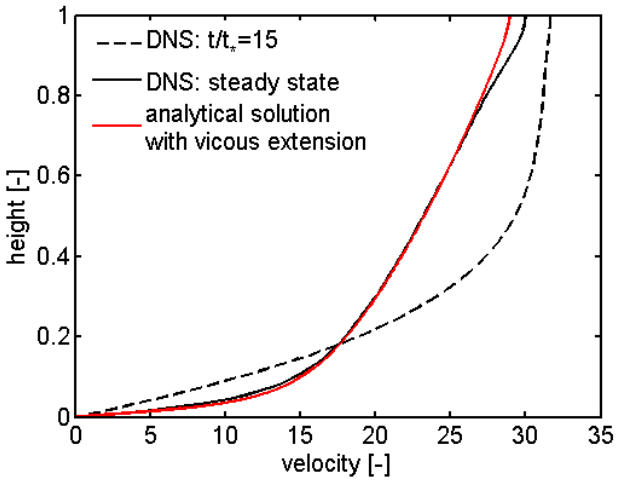

Figure 7. Mean velocity profiles prior and after perturbation for the case $h/L_{ext} = 0.6$. The perturbation is applied at $t/t_* = 15$. Dashed black line: mean velocity profile after collapse of turbulence just before addition of the perturbation; continuous black line: mean velocity profile at $t_* = 40$ i.e. when the new, turbulent steady state has been established; continuous red line: end state as predicted by analytical solution with viscous extension.

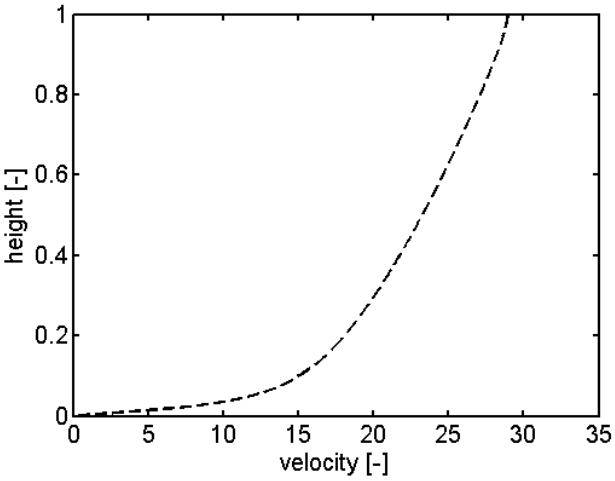

Figure 8. Velocity profile which is used as alternative initial condition with higher shear (compared to the default, neutral initial condition). The profile is taken from the analytical solution (with viscous extension) for the $h/L_{ext} = 0.6$ case as described in section 3.

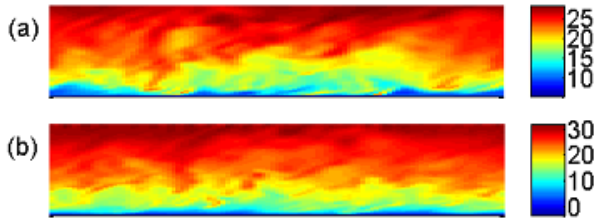

Figure 9. Vertical cross-section of magnitude of the mean velocity field: (a) initial condition: analytical solution for $h/L_{ext} = 0.6$ case with turbulent perturbations added (see text) (b) final state at $t/t_* = 25$. Colours indicate the dimensionless magnitude of the velocity.

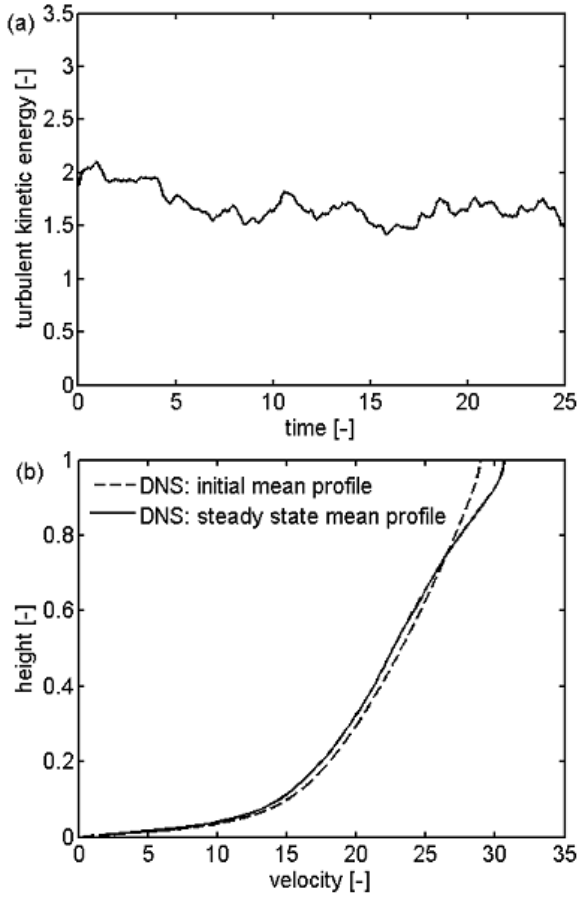

Figure 10. (a) Temporal evolution of the domain-integrated turbulent kinetic energy (b) simulated vertical mean velocity profile at $t/t_* = 25$ (continuous line). The dashed line indicates the initial profile: *viz.* the anticipated analytical steady state solution (see text).